View metadata, citation and similar papers at core.ac.uk
brought to you by CORE
provided by UCrea

*Progress In Electromagnetics Research, Vol. 131, 457–475, 2012*

# CHARACTERIZATION AND MODELING OF SCHOTTKY DIODES UP TO 110 GHz FOR USE IN BOTH FLIP-CHIP AND WIRE-BONDED ASSEMBLED ENVIRONMENTS

**K. Zeljami[1], J. Gutiérrez[1], J. P. Pascual[1], T. Fernández[1, *], A. Tazón[1], and M. Boussouis[2]**

[1]Department of Communications Engineering, University of Cantabria, Edificio I+D+I de Ingeniería de Telecomunicaciones, Plaza de la Ciencia, S/n Santander 39005, Spain

[2]Physics Department, Faculty of Sciences, University of Abdelmalek Essaadi, Tetouan, Morocco

**Abstract**—This paper presents a wideband model, from Direct Current (DC) to W band, for a single Anode Schottky Diode based on a commercial VDI chip. Different measurements have been performed to obtain a complete large-signal equivalent circuit model suitable for the device under consideration up to 110 GHz, and for its integration in planar circuits. The modeling has been done using a combination of DC measurements, capacitance measurements, and RF scattering measurements. The test structure for on-wafer $S$-parameter characterization has been developed to obtain an equivalent circuit for Coplanar to Microstrip (CPW-Microstrip) transitions, then verified with 3D Electromagnetic (EM) tools and finally used to de-embed device measurements from empirical data results in W band. 3D EM simulation of the diodes was used to initialize the parasitic parameters. Those significant extrinsic elements were combined with the intrinsic elements. The results show that the proposed method is suitable to determine parameters of the diode model with an excellent fit with measurements. Using this model, the simulated performance for a number of diode structures has given accurate predictions up to 110 GHz. Some anomalous phenomena such as parasitic resistance dependence on frequency have been found.

*Received 13 July 2012, Accepted 31 August 2012, Scheduled 17 September 2012*
* Corresponding author: Tomas Fernandez (tomas.fernandez@unican.es).

Reproduced courtesy of The Electromagnetics Academy

## 1. INTRODUCTION

The concept of Terahertz Electronics has emerged during the last two decades and draws increasing attention in security applications such as imaging systems [1, 2], security screening systems, genetic engineering, pharmaceutical quality control and medical imaging. In these frequency bands simplicity of non linear devices is required to minimize parasitic effects. Different types of diodes, such as avalanche diodes [3] or Schottky diodes, could be a natural choice.

Particularly Schottky diodes have been widely accepted as a useful solution for Terahertz (THz) applications. These components are used for design of mixers and frequency multipliers in sub-millimeter wavelengths [4]. In addition, the planar diode opens up the possibility of diode circuit integration [5].

The advantages of GaAs Schottky diodes include monopolar operation, high mobility and low noise figures at room temperature. They are presently considered as mature devices, but they are still the subject of investigation concerning their optimization. For operation in millimeter and sub-millimeter wavelength, and for high-frequency applications, n-doped GaAs is the typical semiconductor used in the metal- semiconductor system but the performance of a GaAs Schottky diode is still limited by its parasitic elements [6] and the losses due to skin effects [7]. Moreover, the geometrical design of Schottky diodes is a very critical factor in determining the device performance. Thus, systematic studies of the Schottky diode's parasitic elements and high-frequency losses are very crucial in achieving the design goals.

Generally in RF design, a diode can be modeled as a combination of resistance and capacitance, both bias-dependent. The Schottky diode model consists of both, linear and nonlinear parts. The nonlinear part corresponds to the metal-semiconductor junction, and the linear part contains everything else [4]. The construction of millimeter and sub-millimeter-wave Schottky diode-based circuits relies on valid component models in the design stage. Therefore, no parasitic effects introduced by the diode package elements can be neglected at this frequency, and accurate modeling of them is necessary. Several studies on diode modeling have been performed [8, 9].

In this paper, we describe the characterization of a high-performance Schottky diode for millimeter wavelengths. Model extraction is based on different measurements and computer-aided parameter extraction. The different measurements were: direct current (DC) characteristics, capacitance measurements, scattering (S) parameter measurements and measurements of the assembly of Coplanar to Microstrip bonded transitions used to achieve the complete

Reproduced courtesy of The Electromagnetics Academy

final diode model up to 110 GHz. In accordance with the availability of measurement equipment, the measurements were carried out in two frequency ranges: DC-50 GHz and 75–110 GHz.

## 2. DIRECT CURRENT (DC) CHARACTERIZATION OF SCHOTTKY DIODES

The intrinsic Schottky diode is modeled as a circuit containing four physical parameters [10]: a series resistance $R_s$, a shunt resistance $R_j$, a Schottky diode reverse saturation current Is and a Schottky diode ideality factor $\eta$.

The dominant current transport mechanisms in state-of-the-art GaAs Schottky mixer diodes are the emission of electrons over the barrier and the quantum mechanical tunneling of electrons through the barrier. A widely recognized model which takes into account both of these effects is the thermionic-field emission model [11] generalized I-V characteristics, Equation (1):

$$I(V_d) = I_s \left[\exp\left(\frac{q\left(V_d - I_d R_S\right)}{\eta kT}\right) - 1\right] \approx I_s \exp\left(\frac{q\left(V_d - I_d R_s\right)}{\eta kT}\right) \quad (1)$$

where $I_s$ is the saturation current, $V_d$ is the voltage across the Schottky barrier, $\eta$ is the ideality factor and $R_s$ is the series resistance of the diode.

### 2.1. Extraction of the Resistance, Saturation Current and Ideality Factor

Direct Current (DC) measurements are the most common characterization and testing method for Schottky diodes. This method first performs current-voltage measurements and then facilitates the characterization of the nonlinear properties of the Schottky diode when it is driven into the forward-biased state. In this part, we will perform measurements that will lead us to obtain the parameters characterizing the Schottky junction, which determine the conduction properties of these diodes when the forward bias is applied, and to obtain the parasitic resistance values $R_s$ of the Schottky diode by fitting from the current-voltage measurements [12].

Based on the Schottky diode Equation (1), a voltage-controlled current source is used. The values of the current $I_d$ are injected and the equivalent diode voltage $V$ is measured. The voltage across the Schottky barrier is equal to an applied voltage minus any voltage drop across the series resistance $R_s$ that is, $V_d = V - I \cdot R_s$ and at low levels of polarization when the voltage drop across the series resistance $R_s$ is

Reproduced courtesy of The Electromagnetics Academy

negligible compared to the voltage drop in the space charge region [13], so $V_d = V$;

$$V_d = I_d Rs + \frac{\eta kT}{q} \ln \left[ {}^{I_d}/_{I_s} \right] \tag{2}$$

$$V_d = V = {}^{1}/_{\alpha} Ln \left( {}^{I_d}/_{I_s} \right) \tag{3}$$

Device parameters such as reverse saturation current (Is) and ideality factor $\eta$ can be found on the semilog-scale of the forward characteristic of the diode. They are found to be close to the nominal values provided in the device's datasheet [14]. Typical forward curve Direct Current (DC) Measurements and the data fitted I-V curve are shown as a solid line in Figure 1.

The available literature describing resistance extraction of the Schottky diode is vast; a widely used approach focuses on the DC measurements. Measured I-V characteristics in a range of low voltage are least-square fitted to Equation (3). The result is considered the "ideal" I-V curve without the effect of the series resistance (Figure 2). Regarding the ideal part, the I-V relation maintains a constant slope on a semilog plot, as indicated by the straight line, at higher current levels, however, the voltage drop across the parasitic resistance becomes significant with respect to the diode voltage drop, and the curve deviates from this line.

The variation from the ideal diode performance is easily observed in the Figure 2. This deviation provides the necessary information to allow extraction of the parasitic resistance value. Figure 3 shows the

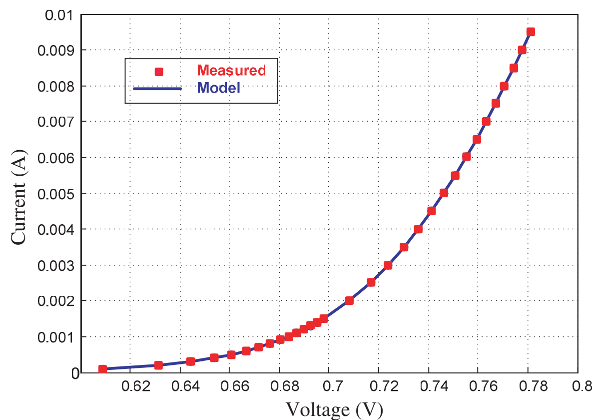


**Figure 1.** Measured and model I-V characteristic results for the Single Anode Schottky Diode.

Reproduced courtesy of The Electromagnetics Academy

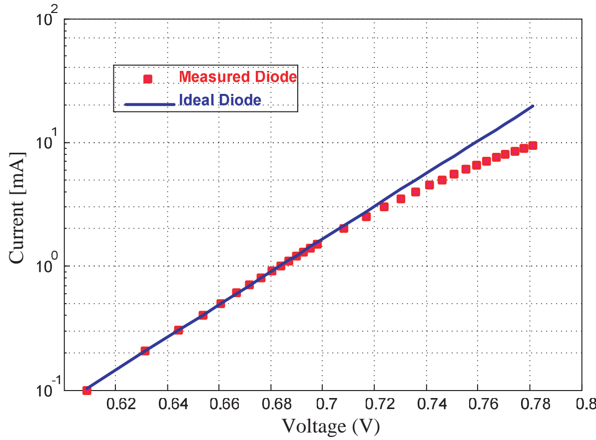


**Figure 2.** Extraction of the series resistances (forward I-V curve of diode plotted with current on logarithmic scale).

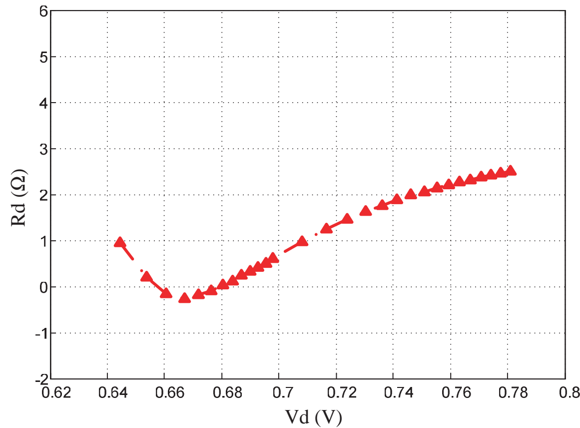


**Figure 3.** Extraction of the series resistance of Single Anode diode (SA-Diode) from measurement voltage.

extraction of the series resistance from voltage measurements. At large voltage values, the resistance increases slightly with increasing voltage, but it remains within the limit values given by the datasheet [14].

## 2.2. Capacitance Extraction

The capacitance of Schottky diodes is the key factor for the high-frequency performance of mixers, detectors or frequency multipliers.

Reproduced courtesy of The Electromagnetics Academy

The usual form for the diode capacitance-voltage relationship, taking into account the dependent junction capacitance, has been given by [15, 16]:

$$C_j(V) = \frac{dQ}{dV} = \frac{C_{j0}}{\left(1 - \frac{V_j}{\phi_{bi}}\right)^{\gamma}} \tag{4}$$

where $C_{j0}$ is the zero-bias junction capacitance, $\Phi_{bi}$ is the built-in potential, $V_j$ is the junction voltage ($V_j > 0$) and the exponent $\gamma$ is a function of the doping profile. The total capacitance of a Schottky diode can be divided mainly into the junction capacitance and the parasitic capacitance. Using Equation (1), the total capacitance can be expressed as:

$$C_{\text{total}} = C_j + C_{pp} = C_j(V) = \frac{C_{j0}}{\sqrt{\left(1 - \frac{V_d}{\phi_{bi}}\right)}} + C_{pp} \tag{5}$$

Several methods have been proposed to determine the junction and parasitic capacitances and built-in voltage [17, 18] of a Schottky diode; in this work apparent capacitance of the diode chips was measured in two ways: from on-wafer $S$-parameter measurements and with low-frequency measurements using a LCR (Inductance-Capacitance-Resistance) meter. Differences between the two methods are compared. The junction capacitance, along with some other capacitance-voltage C-V parameters, is then obtained by fitting the measurement results to a nonlinear capacitance expression (Equation (5)) in a least squares sense.

At lower microwave frequencies, when the diode is not yet conducting, the equivalent circuit of the diode can be reduced to a "$\pi$" network of capacitances [18], formed by the total capacitance $C_T$ and small parasitic capacitances to the ground. $C_T$ is the sum of the junction capacitance $C_{j0}$ and the parasitic capacitances $C_{pp}$. An accurate estimation for the total capacitance can be extracted by fitting the measured value of the transmission coefficient (Figure 4), which is dependent mainly on the total capacitance $C_T$, the ratio between $C_{j0}$ and $C_{pp}$. The $S$ parameters were measured from 2 GHz up to 50 GHz, however, for the capacitance extraction only, the frequency range 3–10 GHz is used, according to the condition for the reduction of the equivalent circuit of the diode to only three capacitances.

The low-frequency measurements have been done using an Agilent E4980A LCR meter. Frequency is set at 1 MHz. Measurements are done on a Single Anode Diode flip-chip mounted on a test structure (Figure 5). The calibration was done by measuring an empty gap

Reproduced courtesy of The Electromagnetics Academy

with the same dimensions as the test structure with the diode; this represents the parasitic capacitance correction for the measurement. Results are illustrated in Figure 6.

Comparing the capacitance curve results shown in Figure 7 for the two capacitance determination techniques based on $S$-parameter measurements and on LCR meter measurements [19], it can be seen that the extracted values for the parasitic capacitance from the LCR meter are greater than those obtained using the $S$-parameter technique. This may be due to the contact of the diode with the test fixture microstrip lines, which can cause the appearance of a large parasitic capacitance and affect the correct measurements of all the extracted capacitance parameters of the diode.

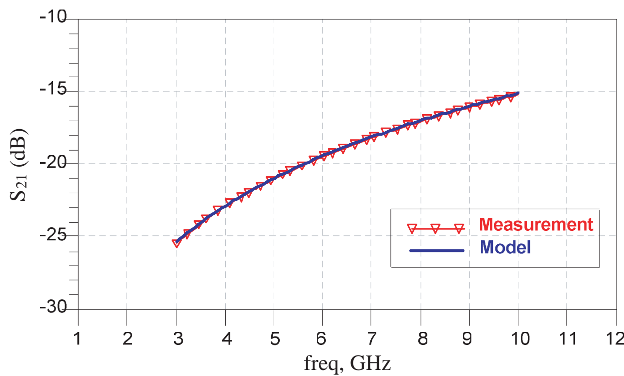


**Figure 4.** Measurement of transmission coefficient and calculated transmission coefficient for the Single Anode Schottky Diode.

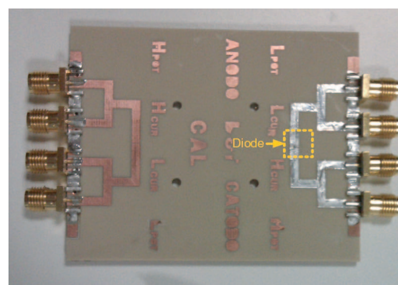


**Figure 5.** Simple test structure, flip-chip mounted discrete diode.

Reproduced courtesy of The Electromagnetics Academy

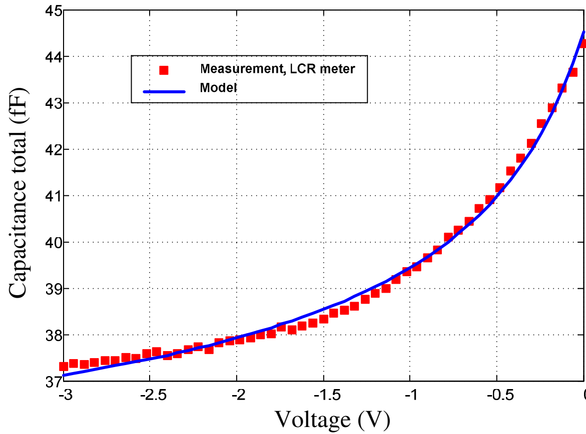


**Figure 6.** C-V Extraction. Equation (5) is fitted to total capacitance values measured with LCR meter.

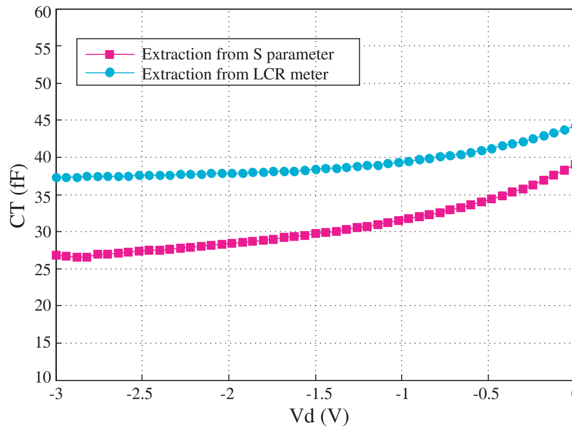


**Figure 7.** Measured and extracted total capacitances and other voltage capacitance parameters, Equation (5) is fitted against measured total capacitance values.

## 3. CHARACTERIZATION OF DIODES: SIMULATION (MODELING TOOLS)

The final goal of the characterization process is to develop a large-signal equivalent circuit of the device. This involves the characterization of both, intrinsic elements and parasitic elements of the device. This part deals with the investigation of the parasitic elements introduced by contacting pad air bridges, bond wires, and semiconductor substrate.

Reproduced courtesy of The Electromagnetics Academy

In this modeling work, suitable design and optimization methods have been implemented on two simulators: a 3D electromagnetic simulator HFSS (Ansoft High Frequency Simulation Software) and a circuit simulator ADS (Agilent Advanced Design System).

Once the significant extrinsic elements have been identified from the diode layer, their values can be determined using two-port measurements. As a starting point, amplitude and phase measurements of the anode reflection coefficient, $S_{11}$, and the anode to cathode transmission coefficient, $S_{21}$, were taken at zero bias. With realistic initial estimates for the elements values based on the physical structure of the device using SEM (Scanning Electron Microscope) image (Figure 8), along with measurements taken from Direct Current DC up to high microwave frequencies; equal weighting was applied to all responses, across the whole frequency range.

A good optimization algorithm produces values that quickly converge to the correct values. When zero bias convergence has taken place, the voltage dependency of $C_j$(v) and $R_j$(v) can be implemented using a SDD (Symbolically-Defined-Device) module from ADS. The error function produced by the optimization algorithm should remain relatively constant for all the potential bias points. Figure 8 shows a Single Anode Diode under consideration. The nominal overall chip dimensions of the diode are 600 µm × 250 µm × 100 µm (length × width × thickness). It is connected with coplanar-to-microstrip transitions (model PROBE POINT TM1003 JmicroTM transition) [20]. This configuration is desirable to enable on-wafer measurements using air coplanar probes, but in this case requires the use of wire bonding connections. This chip connection procedure features low cost, high reliability, and high manufacturability [21].

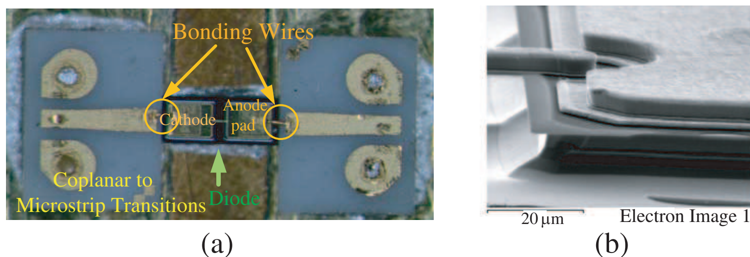


(a) (b)

**Figure 8.** (a) Single Anode Diode (SA-Diode) bonded with gold wires (diameter of 17 µm and length 200 µm–210 µm at both sides). (b) Scanning Electron Microscope (SEM) image of a Single Anode Diode.

Reproduced courtesy of The Electromagnetics Academy

### 3.1. Equivalent Circuit Model of the Diode (Lumped Elements: Intrinsic and Extrinsic)

The equivalent circuit model depends on the type of the diode, and on the surrounding circuitry. Figure 9 shows the equivalent circuit proposed for the discrete planar Schottky diodes under consideration in order to illustrate its integration in a microstrip circuit environment including bonding wires. As with the previous low-frequency models, the distributed resistance and capacitance of the active layer are transformed into a first order equivalent network represented by $R_s$ and $C_j(v)$. The model accommodates forward bias with the junction leakage resistance, $R_j(v)$. This resistance is effectively an open circuit with reverse bias [22].

The circuit includes a finger inductor $L_p$ (estimated using the planar inductor approximation [23]) and a pad-to-pad capacitor $C_{pp}$, which represents the capacitance between the two bonding pads of the diode. In parallel with the Schottky junction is the finger-to-pad capacitance component $C_p$, which represents the capacitance between the anode contact finger and the underlying active GaAs. A set of simple lumped elements models parts inside and outside the diode: an ideal inductance $L_2$ in series with resistor $R$ represents the wire inductance and losses due to the metallization and wire bonding, as well as radiation losses at the wire bends [24, 25]. The two shunt capacitances close to the input and output ports ($C_1$, $C_2$) represent the substrate capacitance between the microstrip lines onto which the wire is bonded. Therefore, they are used to model the discontinuity between the contact lines. The discontinuities on both sides are not necessarily identical since the planar diode structure is not completely symmetric and the length of the bond wires is not exactly the same on both sides. The inductor $L_1$ represents end inductance caused by the wire bonds. Finally, the intrinsic device is represented through its characteristic

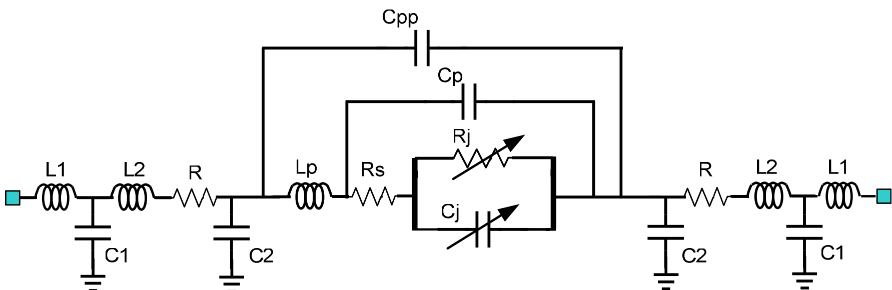


**Figure 9.** Single Anode lumped equivalent circuit for Schottky diode with the extrinsic elements detailed.

Reproduced courtesy of The Electromagnetics Academy

elements: $R_j$ is the nonlinear Schottky junction resistance that acts in parallel with the diode junction capacitance $C_j$, and the ohmic contact resistance is denoted by $R_s$. The equivalent values for each intrinsic element component are extracted from measured Direct Current (DC) characteristics and scattering parameters with fixed RF power levels ($\leq -30\,\text{dBm}$), and the diode unbiased and also reverse biased.

### 3.2. Characterization of Coplanar to Microstrip (CPW-Microstrip) Transitions

Coplanar to Microstrip transitions have been used to measure the diode. The effect of the transitions can be removed from the measurements by applying the calibration proposed by the manufacturer. However, this calibration kit is not intended for the 75–110 GHz band. In this case a generic calibration procedure placing the measurement reference planes at the probe tips is used. Therefore, neither CPW-Microstrip transitions nor wire bonds can be automatically de-embedded and the task of de-embedding parasitic effects of these CPW-Microstrip transitions becomes a new concern. In this sense an electromagnetic model for two CPW-Microstrip transitions connected with a bond wire was developed for this work. This model will be used to de-embed device measurements from empirical data results, which means isolating the performance of the diode by extracting the effect of the transitions from the measurements.

The CPW-Microstrip transitions are attached to a gold plated brass as ground plane using a conductive epoxy and wire bonded to the microstrip part. In this case a calibration using the generic procedure has been performed (Cascade Probe LRM), by placing the measuring planes in the positions (a) and (b) marked in Figure 10. Subsequently, the position of the reference plane may be changed in order to take into

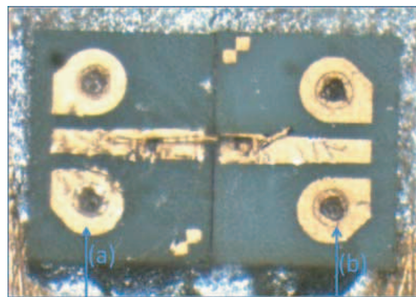


**Figure 10.** The assembly of the two “Coplanar to Microstrip” transitions, connecting with the bond wire.

Reproduced courtesy of The Electromagnetics Academy

account the effects of the two CPW-Microstrip transitions and bond wire. To calibrate the system in the plane of coplanar probes, LRRM calibration (LINE, REFLECT, REFLECT, MATCH) [26], as well as coplanar standards (Cascade Microtech ISS 101-190), have been used. The $S$-parameter measurement of the test sample has been performed using a network analyzer in the 2–50 GHz range and a PNA-X with millimeter-wave head extensions in the W-band.

To validate the response obtained in the measurements carried out, the 3D electromagnetic simulator HFSS (High Frequency Structure Simulator) has been used. In this way, the assembly of the CPW-Microstrip transitions has been performed as is shown in the Figure 11, in order to obtain the behavior of the scattering parameters as a function of frequency as shown in the plots Figure 12. The simulations have been executed from 1 up to 110 GHz. Close fitting is obtained between simulation and measurement.

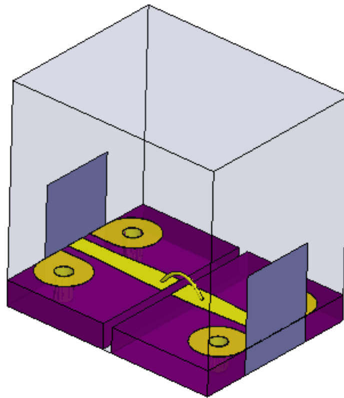

**Figure 11.** 3D view of the assembly of the two transitions, connected with the bond wire.

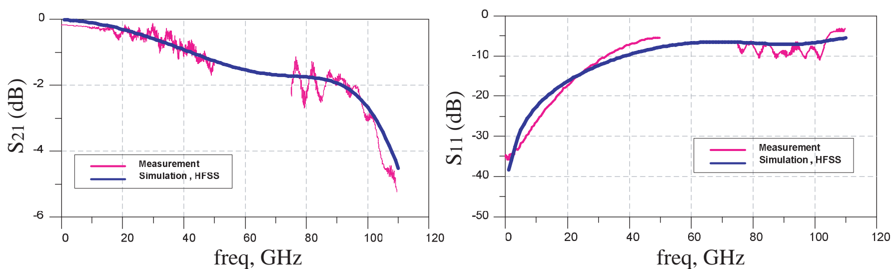


**Figure 12.** Simulation of the assembly of the two transitions, connected with the bond wire.

Reproduced courtesy of The Electromagnetics Academy

### 3.3. Measurement Setup

Before the measurements were made, the system was calibrated at the probe tips using a Cascade probe LRRM (LINE, REFLECT, REFLECT, MATCH) calibration kit. In this way, the measurements are carried out in two different frequency ranges: (1–50 GHz) and in W-band (75–110 GHz), at an ambient temperature of 293 K at several bias voltage points from −3.5 to 0 V. The operation of the measurement set-up has been checked in the first place by measuring in the frequency band 1–50 GHz, using TRL calibration (THROUGH, REFLECT, LINE) to correct the effect of the transitions and to obtain the scattering parameters of the diode with the bond wire in the input and output of the device. A value of −30 dBm of input power has been established to carry out the measurements and reverse biasing has been applied to the diode.

In the frequency band 75–110 GHz, the measurement equipment consists of a microwave network analyzer, N5242A PNA-X, which can only obtain $S$-parameters up to 26.5 GHz. For this reason two external millimeter-wave (VNA-extensions) [27] heads were connected to PNA-X for measuring $S$-parameters in W band. A waveguide to coaxial transition (model 35WR10WF) and 1 mm-coaxial cables, which allow us to measure over the entire W band (75–110 GHz) and finally, coplanar probes (Model 110 H) with a spacing ("pitch") of 125 µm are necessary to measure on-wafer. These measuring tips serve as adapters between the wires and measuring contact surfaces ("Pads") of the structure.

Direct measurements placing a couple of probe tips on the anode and cathode pads were done to verify that coherence of the model is not affected by the surrounding parasitic effects associated with wire bonding and transitions. A special 150 µm pitch differential probe with two contacts (Signal-Ground) was placed just on the pad-to-pad diode gap, as can be seen in Figure 13.

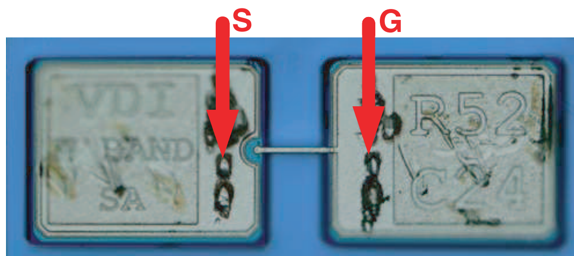


**Figure 13.** Single Anode Diode, measurement with probe (50A-GS-150-P).

Reproduced courtesy of The Electromagnetics Academy

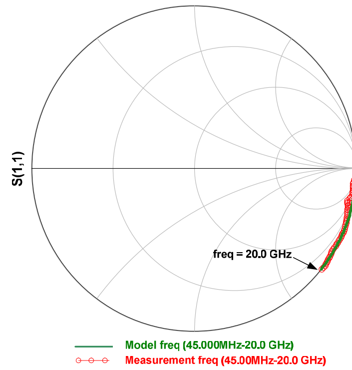


**Figure 14.** Reflection coefficient simulated and measured for Schottky Diode with probe (50A-GS-150-P).

Results have been verified by comparing the reflection parameter, $S_{11}$ (Figure 14), through low frequency diode measurements (up to 20 GHz) with the equivalent circuit model modified for this verification removing the components which represent the test fixture (bonding, Transitions, etc.) and taking into account only grounding capacitance Very good agreement between the measurement and the model was achieved.

## 3.4. Results

$S$-parameter measurements and simulation results at 1–110 GHz for a Coplanar to Microstrip transitions de-embedded Single Anode diode, using the equivalent circuit model shown in Figure 9, are represented in Figure 15, Figure 16. It can be seen from the figures that the equivalent circuit model describes the behavior of the diode well. The reflection and transmission coefficients from the equivalent circuit simulation are represented, first for the unbiased diode (0 V) (Figure 15) and then for the reverse-biased diode (−3 V) (Figure 16). De-embedding of Coplanar to Microstrip transitions in W band was done using ADS.

It should be noted here that our model takes into account the increase of the wire bonding series resistance caused by the skin effect [25] at frequencies above 50 GHz and eventually by some other measurement uncertainties. The study of the extent of this effect becomes difficult at this frequency band, as measurements are limited by calibration accuracy and some possible inaccuracy in the determination of other equivalent circuit parameters such as finger inductance, parasitic capacitances, etc.. Nevertheless, the increase in resistance in W band was consistently found when fitting measurements of several devices. The resulting extracted model parameters are listed in Table 1.

Reproduced courtesy of The Electromagnetics Academy

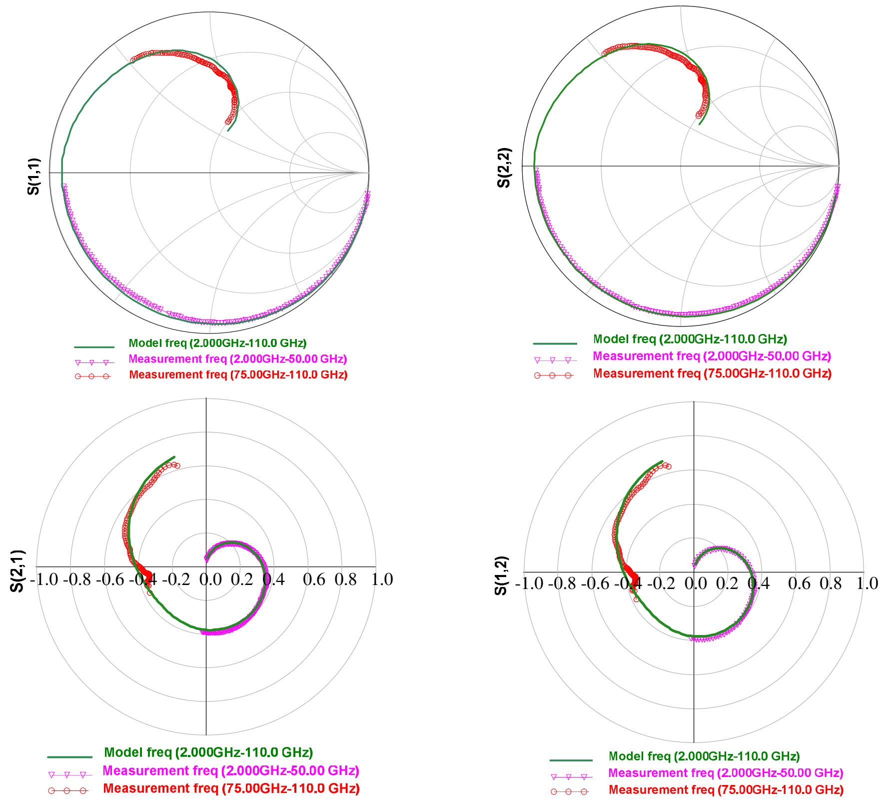


**Figure 15.** $S$-parameter simulation and measurement for Schottky Diode using circuit in Figure 9. Diode is unbiased (0 V).

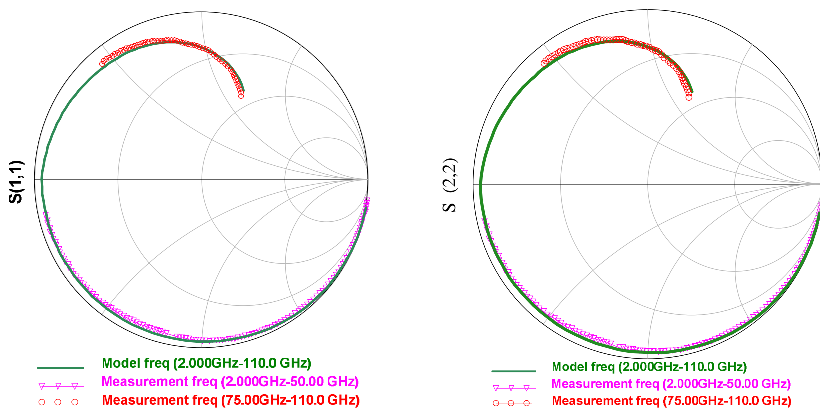


Reproduced courtesy of The Electromagnetics Academy

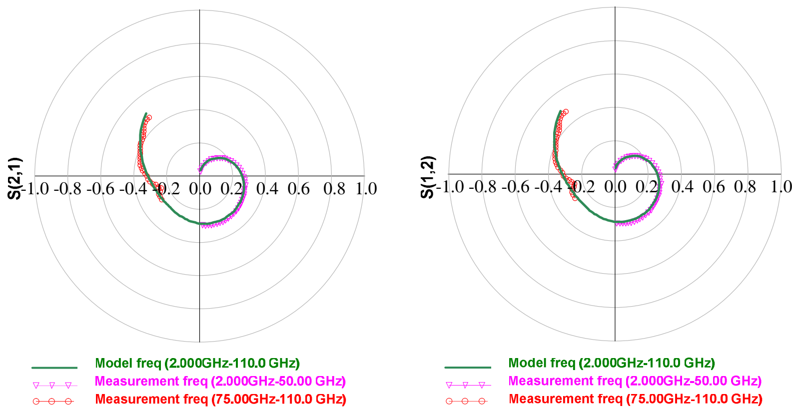


**Figure 16.** $S$-parameter simulation and measurement for Schottky Diode using circuit in Figure 8. Diode was biased ($-3$ V).

**Table 1.** Extracted parameters of the Schottky diode under consideration.

| **Parameters** | **Symbol** | **Value** |
|---|---|---|
| Saturation current (A) | $I_{\text{sat}}$ | $9.97593 \cdot 10^{-13}$ |
| Ideality factor | $\eta$ | 1.28 |
| nkT/q (1/V) | $\alpha$ | 30.31 |
| Zero junction capacitance (fF) | $C_{j0}$ | 24 |
| Series resistance (Ω) | $R_s$ | 2.4429 |
| Built-in-potential (V) | $\phi_{bi}$ | 0.9 |
| Finger inductance (pH) | $L_p$ | 50 |
| Parasitic capacitance (fF) | $C_p$ | 1 |
| Pad-to-pad capacitance (fF) | $C_{pp}$ | 15 |
| Bonding inductance (pH) | $L_1$ | 60.13 |
| Bonding inductance (pH) | $L_2$ | 51.36 |
| Pad capacitance (fF) | $C_1$ | 60.34 |
| Pad capacitance (fF) | $C_2$ | 46.26 |
| Bonding resistance (Ω) | $R$ | 0–3 |

## 4. CONCLUSION

In this work, we have described a procedure for characterizing planar Schottky diodes, based on Direct Current (DC) measurement, capacitance measurements and $S$ parameter measurements, whose results are used to find the equivalent large-signal model of Schottky

Reproduced courtesy of The Electromagnetics Academy

diodes. These diodes have one of the best price-performance ratios on the market and we feel that they will become an integral part of many applications.

The capability of our characterization and modeling method has been demonstrated to create a reliable equivalent circuit model of Schottky diodes with very good accuracy and valid under large signal conditions and at high frequencies up to 110 GHz. This was demonstrated using measurements up to 50 GHz and between 75 GHz and 110 GHz, although with a lack of measurements in the 50–75 GHz range.

Scattering measurements have also been obtained for the assembly of Coplanar to Microstrip transition-bond wire-Coplanar to Microstrip transition to verify the feasibility of the proposed model used for de-embedding. Simulation and measurements of the assembly indicates that the proposed model can describe the behavior of Coplanar to Microstrip transitions well and it can be used to separate the true performance of the diodes from the effect of the elements used in our test fixture.

The model was tested under various bias points and results were compared to the measured data. In all cases, the simulation results are shown to be in good agreement with the measured data. Finally, the model can be easily implemented in any circuit simulator and applied to other types of diodes.

## ACKNOWLEDGMENT

The authors would like to thank the Spanish Ministries of Science and Innovation (MICINN) and of Economy and Competitiveness (MINECO) for the financial support provided through projects CSD2008-00068, TEC2011-29264-C03-01 and FEDER co-funded TEC2011-29126-C03-01. The authors express their gratitude to the Spanish Agency AECI though its program 'Becas para Extranjeros No Iberoamericanos para Estudios de Postgrado, Doctorado y Postdoctorado en Universidades y Centros Superiores en España'. The authors also would like to thank Sandra Pana, Ana Pérez and Eva Cuerno for their help with the assembly of the devices and Dermot Erskine for the correction of the text.

## REFERENCES

1. Yeom, S., D. Lee, H. Lee, J. Son, and V. P. Guschin, "Distance estimation of concealed objects with stereoscopic

Reproduced courtesy of The Electromagnetics Academy

passive millimeter-wave imaging," *Progress In Electromagnetics Research*, Vol. 115, 399–407, 2011.

2. Oka, S., H. Togo, N. Kukutsu, and T. Nagatsuma, "Latest trends in millimeter-wave imaging technology," *Progress In Electromagnetics Research Letters*, Vol. 1, 197–204, 2008.
3. Zhao, M., Y. Fan, D. Wu, and J. Zhan, "The investigation of W band microstrip integrated high order frequency multiplier based on the nonlinear model of avalanche diode," *Progress In Electromagnetics Research*, Vol. 85, 439–453, 2008.
4. Zhan, M. Z., W. Zhao, and R. M. Xu, "Design of millimeter-wave widband mixer with a novel IF bloc," *Progress In Electromagnetics Research C*, Vol. 30, 41–52, 2012.
5. Arboli, M. R.-G., "Monolithic integration of non linear circuits for terahertz applications," Ph.D. Thesis, University of Darmstadt, Shaker Verlag, 2003.
6. Crowe, T. W., "GaAs Schottky barrier mixer diodes for the frequency range 1–10 THz," *International Journal of Infrared and Millimeter Waves*, Vol. 10, 765–777, Jul. 1989.
7. Bhaumik, K., B. Gelmont, R. Mattauch, and M. Shur, "Series impedance of GaAs planar Schottky diodes operated to 500 GHz," *IEEE Transactions on Microwave Theory and Techniques*, Vol. 40, 880–885, 1992.
8. Xu, H., G. S. Schoenthal, L. Liu, Q. Xiao, J. L. Hesler, and R. M. Weikle, "On estimating and canceling parasitic capacitance in submillimeter-wave planar Schottky diodes," *IEEE Microwave and Wireless Components Letters*, Vol. 19, 807–809, 2009.
9. Tang, A. Y., V. Drakinskiy, P. Sobis, J. Vukusic, and J. Stake, "Modeling of GaAs Schottky diodes for terahertz application," *34th International Conference on Infrared, Millimeter, and Terahertz Waves*, Busan, Korea, 2009.
10. Torrey, H. C. and C. A. Whitmer, *Crystal Rectifiers*, MIT Radiation Lab. Series, No. 15, McGraw Hill, New York, 1948.
11. Sze, S. M. and K. K. Ng, *Physics of Semiconductor Devices*, John Wiley & Sons Inc., Hoboken, NJ, USA, 2007.
12. Golio, J. M., *Microwave MESFETs and HEMTs*, 1991.
13. Fernández, T., "Diseño de un sistema experimental automático para la caracterización DC Y pulsada de transistores de alta frecuencia," Masters Dissertation University of Cantabria, Santander, Oct. 1991.
14. www.virginiadiodoes.com.
15. Sze, S. M., *Semiconductor Devices Physics and Technology*, 2nd

Reproduced courtesy of The Electromagnetics Academy

Edition, John Wiley & Sons, Inc., 2002.

16. Maas, S. A., *Microwave Mixers*, 2nd Edition, Artech House, Inc., 1993.
17. Palmer, D. W., "Characterisation of semiconductors by capacitance methods," *Growth and Characterisation of Semiconductors*, 187–224, A. Hilger, 1990.
18. Kiuru, T., K. Dahlberg, J. Mallat, A. V. Räisänen, and T. Närhi, "Comparison of low-frequency and microwave frequency capacitance determination techniques for mm-wave Schottky diodes," *European Microwave Integrated Circuits Conference (EuMIC)*, Manchester, UK, Oct. 10–11, 2011.
19. Möttönen, V. S., J. Mallat, and A. V. Räisänen, "Characterisation of European millimetre-wave planar diodes," *European Microwave Conference*, 921–924, Amsterdam, The Netherlands, Oct. 12–14, 2004.
20. ProbePoint 1003, "Test interface circuit-coplanar to microstrip," Jmicro Technology.
21. Tummala, R. and E. Rymaszuweski, *Microelectronics Packaging Handbook*, Van Nostrand Reinhold, 1989.
22. Lucyszyn, S., G. Green, and I. D. Robertson, "Accurate millimeter-wave large signal modeling of planar Schottky varactor diodes," *IEEE MTT-S International on Microwave Symposium Digest*, Vol. 1, 1992.
23. Greenhouse, H., "Design of planar rectangular microelectronic inductors," *IEEE Transactions on Parts, Hybrids, and Packaging*, Vol. 10, No. 2, 101–109, Jun. 1974.
24. Jahn, D., R. Reuter, Y. Yin, and J. Feige, "Characterization and modeling of wire bond interconnects up to 100 GHz," *IEEE on Compound Semiconductor Integrated Circuit Symposium, CSIC*, 111–114, Nov. 2006.
25. Lee, H.-Y., "Wideband characterization of a typical bonding wire for microwave and millimeter-wave integrated circuits," *IEEE Transactions on Microwave Theory and Techniques*, Vol. 43, No. 1, Jan. 1995.
26. Purroy, F. and L. Pradell, "New theoretical analysis of the LRRM calibration technique for vector network analyzers," *IEEE Transactions on Instrumentation and Measurement*, Vol. 50, No. 5, 1307–1314, Oct. 2001.
27. http://www.omlinc.com/products/vna-extension-modules/wr-10-75-110-ghz.html.

Reproduced courtesy of The Electromagnetics Academy